RSC Advances

PAPER

View Article Online
View Journal | View Issue

Cite this: *RSC Adv.*, 2024, **14**, 1034

Portable glucose sensing analysis based on laser-induced graphene composite electrode

Zhaokang Zhang,[a] Lu Huang,[b] Yiting Chen,[b] Zhenli Qiu,[b] Xiangying Meng*[c] and Yanxia Li *[b]

In this work, a portable electrochemical glucose sensor was studied based on a laser-induced graphene (LIG) composite electrode. A flexible graphene electrode was prepared using LIG technology. Poly(3,4-ethylene dioxythiophene) (PEDOT) and gold nanoparticles (Au NPs) were deposited on the electrode surface by potentiostatic deposition to obtain a composite electrode with good conductivity and stability. Glucose oxidase (GOx) was then immobilized using glutaraldehyde (GA) to create an LIG/PEDOT/Au/GOx micro-sensing interface. The concentration of glucose solution is directly related to the current value by chronoamperometry. Results show that the sensor based on the LIG/PEDOT/Au/GOx flexible electrode can detect glucose solutions within a concentration range of 0.5×10^{-5} to 2.5×10^{-3} mol L^{-1}. The modified LIG electrode provides the resulting glucose sensor with an excellent sensitivity of 341.67 μA mM^{-1} cm^{-2} and an ultra-low limit of detection (S/N = 3) of 0.2×10^{-5} mol L^{-1}. The prepared sensor exhibits high sensitivity, stability, and selectivity, making it suitable for analyzing biological fluid samples. The composite electrode is user-friendly, and can be built into a portable biosensor device through smartphone detection. Thus, the developed sensor has the potential to be applied in point-of-care platforms such as environmental monitoring, public health, and food safety.

Received 12th October 2023
Accepted 12th December 2023

DOI: 10.1039/d3ra06947h

rsc.li/rsc-advances

1 Introduction

Diabetes is a chronic metabolic disease with systemic effects that can lead to multiple complications and even death. According to the World Health Organization, more than 400 million individuals worldwide have diabetes, highlighting its status as a significant global public health threat (WHO, 2022). As a result, there is an urgent need for millions of diabetics to have access to simple, sensitive, and user-friendly glucose sensors capable of detecting blood glucose levels.[1,2] The conventional approach to glucose detection involves blood detection, which necessitates a large number of blood samples, resulting in inconvenience to certain groups, such as children, the elderly, or patients with blood coagulation disorders. Furthermore, the sample processing time is lengthy, the procedure is complicated, and professional detection equipment and technicians are required.[3] Consequently, there is an urgent need to develop a rapid, straightforward, precise, and portable non-invasive glucose detection method. The advent of smartphones has presented a new approach for the development of electrochemical biosensors. Combining smartphones with various biosensors such as heart rate sensors, blood pressure sensors, and blood sugar sensors can enable individuals to monitor their physical health in real-time and take prompt action.[4,5]

Graphene is a sp^2 hybrid carbon nanosheet that offers high conductivity, specific surface area, and biocompatibility, making it a popular choice in biosensing devices. Methods used for preparation include mechanical stripping, chemical vapor deposition, and redox methods, which all have significant drawbacks, including high costs, long preparation times, and environmental pollution, which limit large-scale manufacturing.[6,7] However, laser-induced graphene (LIG) technology is a promising alternative as it uses laser irradiation on a PI surface, causing rapid temperature increases that break C–O, C=O, and N–C bonds and release CO, C_2H_2, and other gases. This process rearranges aromatic groups, transforming sp^3 hybrid carbon atoms into sp^2 hybrid carbon atoms and creating the basic structure of graphene, allowing for rapid preparation at a low cost.[8,9] Composites that incorporate graphene, conductive polymers, and metal nanoparticles offer improved performance and expand the range of applications for these materials. Graphene/conductive polymer/metal nanoparticle composites can detect a variety of compounds and molecules such as glucose, urea, protein, and DNA,[10–14] indicating promising prospects in the field of biosensing.

PEDOT is a conjugated polymer synthesized from 3,4-ethylene dioxythiophene (EDOT) monomer that exhibit excellent electrical conductivity and have been proven to enhance the

[a]College of Chemical Engineering, Fuzhou University, Fuzhou, 350108, China
[b]College of Materials and Chemical Engineering, Minjiang University, Fuzhou, 350108, China. E-mail: yxli09@163.com
[c]School of Medical Laboratory, Weifang Medical University, Weifang, 261053, China

electrochemical performance of biosensing electrode.[15,16] Depositing of a PEDOT film on the LIG electrode surface *via* a potentiostatic method can enhance the mechanical properties, hydrophilicity and anti-pollution performance of LIG.[17] Additionally, enzymatic oxidation-based amperometric glucose sensors utilizing electroactive noble metals (*e.g.*, gold and platinum) have garnered increasing attention. Among them, gold nanoparticles exhibit exceptional performance in enzymatic electrochemical biosensing, owing to their stable chemical properties, good biocompatibility, good electrical conductivity, and high catalytic activity.[18] Incorporating gold nanoparticles onto the LIG composite electrode surface can increase active sites, enhance the amount of immobilized enzyme, and improve the amperometric response range of the sensor.

As one of the important indicators of human health, glucose detection has always been a research hotspot. Investigators are committed to seeking cheaper, more accurate, minimal or non-invasive methods to quantify glucose levels in real-time. The detection of glucose concentration can be carried out through methods such as chromatography, spectroscopy, and electrochemical analysis. Electrochemical glucose sensors, which have the advantages of low detection cost, high reliability, and strong operability, have attracted much attention and have been widely studied and reported.

In recent years, with the rapid development of intelligent wearable devices, new requirements and heights have been put forward for the development and application of biosensors.[19] Flexible wearability, real-time monitoring, and high stability have become important directions for the development of glucose sensor applications. Flexible wearable devices are gradually improving human life through intelligence, personalization, and convenience, and the related market demand is also constantly increasing. Although the number of components that make up a flexible electrochemical sensor may vary depending on the specific application, it typically includes: substrate unit, sensing unit, decision-making unit, and energy supply unit. Flexible film is a common substrate form, such as polyethylene terephthalate (PET), polyimide (PI).[20] PET and PI have almost no stretchability, making them suitable for fixation in areas where the skin is not easily deformed. Fabric has outstanding advantages in breathability and wear comfort, making it a more ideal substrate material for wearable devices.

The field of fabrication methods for functional circuits on 3D freeform surfaces and standalone stretchable sensing platforms is rapidly evolving. Researchers are continuously exploring new materials, fabrication techniques, and design strategies to overcome challenges related to mechanical durability, electrical performance, and integration of complex functionalities.[21,22] For example, additive manufacturing involves using the techniques of 3D printing or inkjet printing to directly fabricate conductive traces and components on 3D surfaces. It allows for the creation of complex circuit geometries on irregular or curved objects.[23–26] Utilizing stretchable materials as the base substrate for the circuit is a popular approach. These substrates, often made of polymers or elastomers, can deform and stretch without compromising the functionality of the circuit.[27] Serpentine or meandering interconnect designs can accommodate the mechanical deformation of the substrate while maintaining electrical connectivity. Moreover, using methods of stamping or lamination transferred circuit components onto the 3D freeform surface.[28]

The sensing unit is the core component of flexible electrochemical sensors. According to the different detection mechanisms, electrochemical glucose sensors can be divided into non-enzymatic sensors and enzyme-based sensors. The non-enzymatic glucose sensor does not require direct use of enzymes during the detection process, so it is expected to achieve glucose detection under broader conditions. However, conventional non-enzymatic sensors usually cannot respond specifically to glucose molecules, making detection results more susceptible to interference. Relatively speaking, enzymatic glucose sensors typically have higher specificity. However, its detection performance is severely constrained by factors such as the effective load of enzymes and enzyme activity that led to poor reproducibility and stability during use. Therefore, exploring modified methods of electrodes with good performance electrode for obtaining stable binding and high GOx loading has extremely high practical significance. In addition to typical enzymes, the active catalytic materials of glucose sensors are mainly composed of polymers, metals, alloys, metal compounds, and other substances that can catalyze the oxidation of glucose.[29] LIG electrodes have been widely developed due to their excellent biocompatibility, flexibility, pattern-ability, and ability to serve as a favorable environment for enzymes and promote electron transfer.[30] The core of a decision-making unit is a microcontroller unit (MCU), which converts electrical signals into digital signals through components such as signal transduction, amplification units, and analog-to-digital converters. Currently, mainstream electrochemical sensors are applied relatively independently to a single individual, using selected features to perform predefined tasks. Smartphones can easily achieve portability and real-time detection.[31] With the development of machine learning technology, flexible electrochemical sensors are expected to obtain a large amount of physiological information, and create a high-dimensional and multi-level database through distributed sensing unit arrays.[32,33] Traditional energy supply units typically use commercial batteries directly, posing potential risks to the health of patients. Researchers have designed and developed various new wearable energy supply units to meet the demand for flexible and intelligent wearability, such as supercapacitor, triboelectric effect, biofuel cells, *etc.* Mercier *et al.* provide a self-powered model that utilizes glucose biofuel cells as energy sources to obtain energy from glucose in the intestine and measure glucose concentration.[34]

The aim of this study is to develop a portable glucose sensor based on patterned LIG composite electrode. To achieve this, PEDOT and Au NPs are deposited alternatively through a potentiostatic method, and GOx is then immobilized onto the surface of the composite electrode *via* chemical crosslinking. The resulting LIG/PEDOT/Au/GOx glucose biosensing interface demonstrates excellent specificity in catalyzing glucose molecules, which are converted along with oxygen in the substrate to

gluconic acid and hydrogen peroxide, resulting in electron transfer on the electrode surface, and the electrochemical signals changes during this reaction process are recorded for glucose detection. What's more, the LIG/PEDOT/Au/GOx glucose biosensing interface can be combined with portable electrochemical workstation and smartphones to detect actual samples, expanding its potential applications.

2 Experimental

2.1 Instruments and reagents

The LIG electrode preparation was carried out using a Nano Pro-III laser printer manufactured by Tianjin Jiayin Nanotechnology Co., Ltd. The printer is equipped with a continuous semiconductor laser that emits at a wavelength of 450 nm and has an output power of 5.5 W. A portable electrochemical workstation (Sensit/BT) was purchased from Plamsens China Co., Ltd.

Polyimide (PI) film, with a thickness of 0.08 μm, was acquired from Tianjin Jiayin Nanotechnology Co., Ltd. Meanwhile, polyethylene terephthalate (PET) substrate with a thickness of 180 μm was obtained from Nanjing Xianfeng Nanotechnology Co., Ltd. The conductive silver paste and Ag/AgCl paste were purchased from Shenzhen Ausbon Co., Ltd. and Guangzhou Yinbiao Trading Co., Ltd., respectively. Glutaraldehyde (GA) (50%) was obtained from Fuzhou Xinyuhua Experimental Instrument Co., Ltd. Glucose oxidase (GOx) with a specific activity of 248.88 U mg^{-1} was purchased from Sigma-Aldrich (Shanghai) Trading Co., Ltd., while bovine serum albumin (BSA) with a purity of 98.0% was acquired from Beijing Dingguo Biotechnology Co., Ltd. Additionally, artificial sweat (ISO 105/E04 pH 7.0), artificial urine, and fetal bovine serum were obtained from Yuanye Biotechnology Co., Ltd. 11-Mercaptoundecanoic acid (MUA), 3,4-ethylene dioxythiophene (EDOT) with a purity of 99%, and phosphate buffer solution (PBS) with a concentration of 0.1 mol L^{-1} and pH of 7.0 were all purchased from Aladdin Reagent (Shanghai) Co., Ltd. Chloroauric acid tetrahydrate ($HAuCl_4 \cdot 4H_2O$) with a concentration of 47.8% was acquired from Sinopharm Chemical Reagent Co., Ltd. Furthermore, potassium chloride, potassium ferricyanide, glucose, trisodium citrate, and other reagents were of analytical pure grade. Ultrapure water with a resistivity of 18.2 MΩ was obtained using a Millipore Autopure WR600A system (Millipore Ltd., USA) and used in all experiments.

2.2 Preparation of LIG electrode

The PI film should be securely affixed to the PET substrate to facilitate the printing of the three-electrode pattern using the Nano Pro-III laser printer, with settings of 35% relative laser intensity and 20% engraving depth. The graphene three-electrode pattern should be rinsed sequentially with ethanol and water, and then allowed to air dry at room temperature. The end of the three electrodes should be coated with conductive silver paste, while the other end of the reference electrode should be coated with Ag/AgCl paste. The working area was fixed with PI film, and then keep sealed and storage in a refrigerator at 4 °C.

2.3 Preparation of LIG/PEDOT/Au electrode

The mixed aqueous solution of 0.02 mol per L EDOT monomer and 0.02 mol per L trisodium citrate was prepared as the PEDOT deposition solution. It was dissolved completely by magnetic stirring. Meanwhile, a 1% (w/w) chloroauric acid solution containing 0.1 mol per L Na_2SO_4 was also prepared to deposit Au NPs. The Ag/AgCl electrode was used as the reference electrode, the platinum wire as the counter electrode, and the LIG electrode was electrodeposited at a constant potential of 1.1 V for 300 seconds in the PEDOT deposition solution. After washing the surface of the LIG/PEDOT electrode with pure water and drying it, the electrode was placed in the Au NPs deposition solution. The LIG/PEDOT/Au electrode was obtained after 200 s of deposition at a potential of −0.6 V, and it was washed with pure water and dried in air for later use.

2.4 Preparation of LIG/PEDOT/Au/GOx electrode

A 5 mM solution of MUA was prepared by mixing anhydrous ethanol and deionized water in a volume ratio of 6 : 4. Subsequently, 5 μL of the MUA solution was dripped onto the working area of the LIG/PEDOT/Au electrode, followed by a 30 minute incubation period, rinsing with pure water, and drying in air. Refer to our previous research,[35] aqueous solution with final concentration of 4 mg per mL GOx and 2 mg per mL BSA was prepared as the GOx solution. Next, a mixed solution of GOx and GA (diluted to 2% in pure water with a volume ratio of 7 : 3) was dropped onto the surface of LIG/PEDOT/Au electrode, which was activated overnight at 35 °C, rinsed with pure water and dried naturally. Finally, the LIG/PEDOT/Au/GOx electrode keep sealed in a refrigerator at 4 °C and then activated at 35 °C for 10 min before use.

2.5 Electrochemical sensing analysis of glucose

The electrochemical signals were recorded *via* chronoamperometry at a constant potential of 0.9 V using a PalmSens4 portable electrochemical workstation. To generate *i–t* step curves, glucose solutions with varying concentrations (100 μL each) were sequentially added to the system in an increasing order of concentration.

2.6 Biological sample analysis

After the biological samples of fetal bovine serum (FBS) were diluted 20 times, artificial urine and artificial sweat diluted 1 time by PBS, glucose solutions in different biological samples with final concentrations of 0.5×10^{-5}, 2.5×10^{-4} and 1.0×10^{-3} mol L^{-1} were obtained. According to the above electrochemical sensing analysis, the recovery rates of glucose in actual samples (FBS, urine and sweat) with different concentrations of glucose were measured by chronoamperometry.

2.7 Smartphone sensing analysis

The Android smartphone equipped with PSTouch 2.7 App was connected to the SenSit Smart U disk electrochemical analyzer through a Type-C interface. The LIG/PEDOT/Au/GOx electrode was immersed in various glucose solution of biological samples

and inserted into SenSit electrochemical analyzer. Chronoamperometry was adopt under 0.9 V constant potential for 500 s to obtain *i*–*t* curves.

3 Results and discussion

3.1 Glucose sensing strategy using enzyme electrodes

The glucose biosensor described in this paper comprises four main steps: (1) preparation of a bare LIG electrode, (2) electrodeposition a layer-by-layer self-assembled LIG/PEDOT/Au electrode, (3) enzyme modification, (4) and portable detection. The preparation of composite electrodes and glucose sensing strategy is depicted in Scheme 1. Laser-induced 3D porous patterning of graphene on PI was achieved at room temperature through continuous semiconductor lasers, which enabled high-precision preparation of LIG electrode without using harmful chemical reagents and is favorable for developing green, low-cost and high conductivity sensor devices.[36,37] Next, 3,4-ethylene dioxythiophene (EDOT) monomers were electrochemically polymerized on the surface of LIG electrode to form a PEDOT film. As a polymer material with excellent conductivity, deformability and biocompatibility, PEDOT can effectively protect the mesoporous structure of graphene 3D space, and enhances the conductivity and flexibility of electrodes. The deposition of Au NPs on the PEDOT surface can improve the conductivity of the electrode, facilitate the introduction of carboxyl groups through MUA, and facilitate enzyme immobilization. Glutaraldehyde (GA), as a stable bifunctional crosslinking agent, can effectively link the enzyme with biological macromolecules,[38] forming a stable crosslinking structure (–GOx and –GOx, –GOx and –BSA, –BSA and –BSA) that covers the electrode surface. Furthermore, the carboxyl group from MUA can form a hydrogen bond with the carboxyl group of GOx, promoting further enzyme immobilization.[39] BSA blocks unbound active sites to form an antifouling interface.[40,41] The fabricated LIG/PEDOT/Au/GOx micro sensing electrode, in combination with smartphone device, enables data visualization and improves the applicability for self and home-based healthcare management of diabetic patients. This is essential for prolonging the time of clinical diagnosis, both indoors and outdoors.[42]

3.2 Characterization of electrode materials

Scanning electron microscopy (SEM, SU8000) was used to characterize the changes in surface morphology during the electrode assembly process. The results are presented in Fig. 1. The 3D mesoporous structure of LIG electrode effectively improves its surface area, as seen in Fig. 1A and B. In Fig. 1C and D, a thin film covers the porous structure surface, indicating the successful deposition of PEDOT. As can be seen from Fig. 1E and F, the mesoporous structure of graphene remains intact on the electrode surface after electrochemical deposition of Au NPs. The uniform distribution of nanoparticles adhered to the inner wall of large mesoporous structures suggests the successful deposition of Au NPs onto the electrode surface, resulting in the formation of the LIG/PEDOT/Au composite electrode. The spatial structure layer of the LIG/PEDOT/Au/GOx (BSA) composite electrode (Fig. 1G and H) is visibly thicker due to the formation of a cauliflower-like, stable crosslinking layer formed by the tight coating of GA-activated GOx and BSA on the electrode surface.

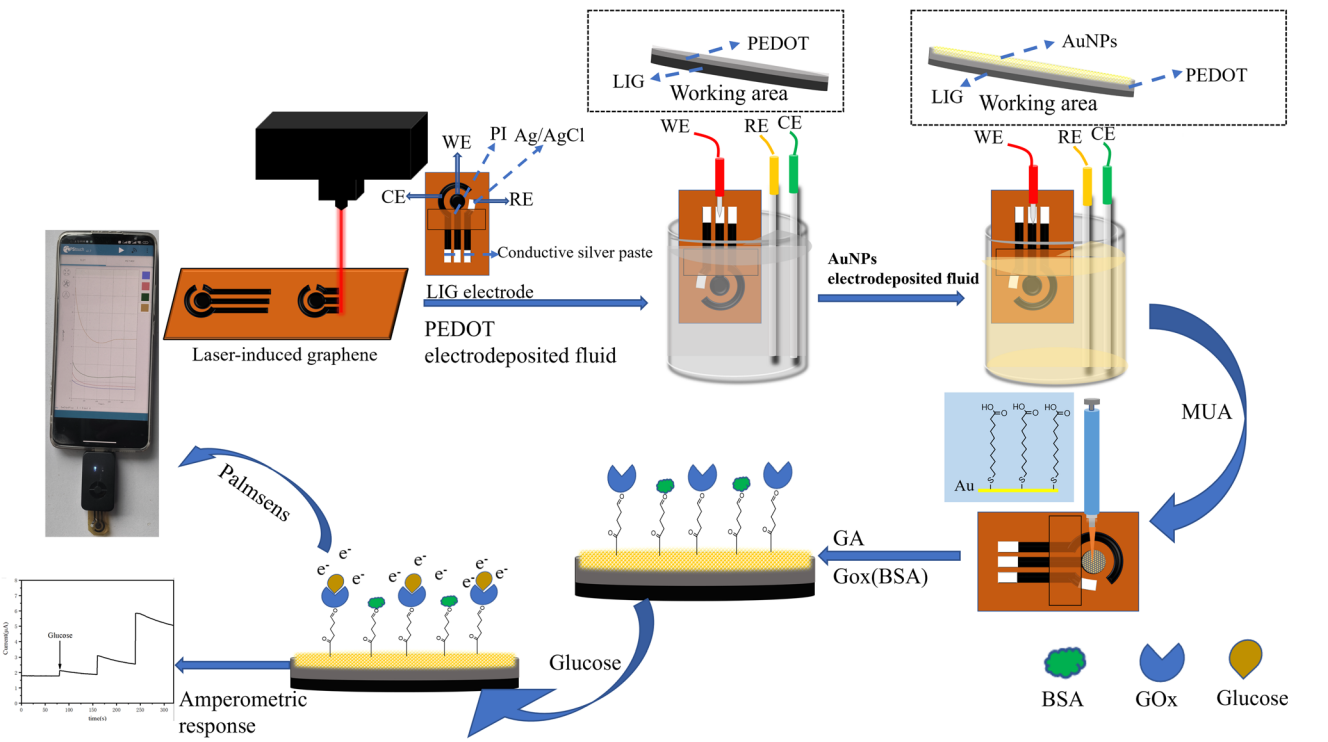

Scheme 1 Schematic of glucose sensing analysis.

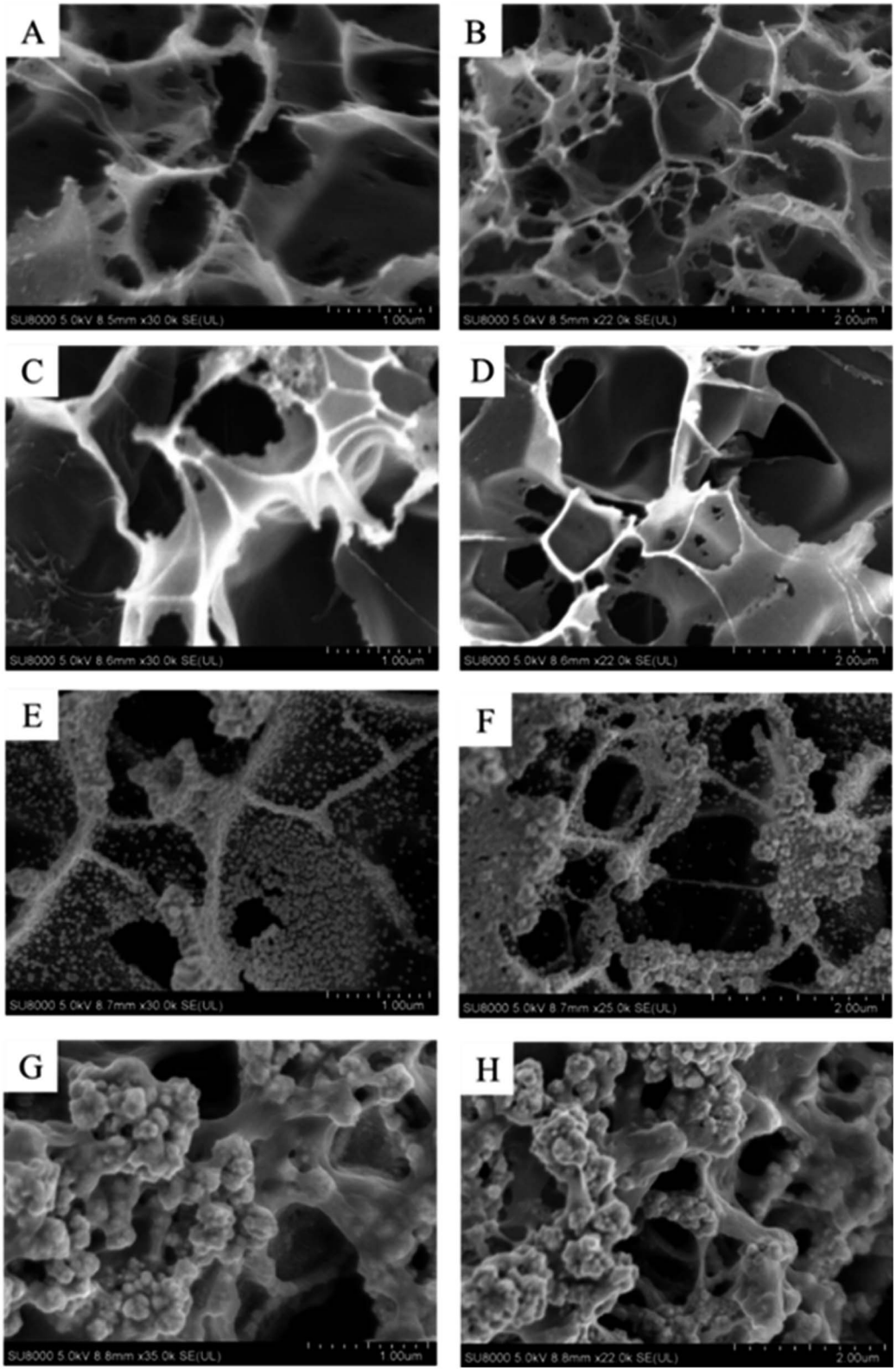

Fig. 1 Scanning electron microscope (SEM) images of bare LIG (A and B) and LIG/PEDOT (C and D), LIG/PEDOT/Au (E and F), LIG/PEDOT/Au/GOx (BSA) (G and H) composite electrodes.

The energy dispersive spectrometer (EDS) was used to analyze changes in surface element content of the modified electrodes for further verification of the electrode assembly process. As shown in Fig. 2A, the surface of the PI film after laser printing was rich in C element, indicating a high degree of graphitization. The laser printing process was carried out in an

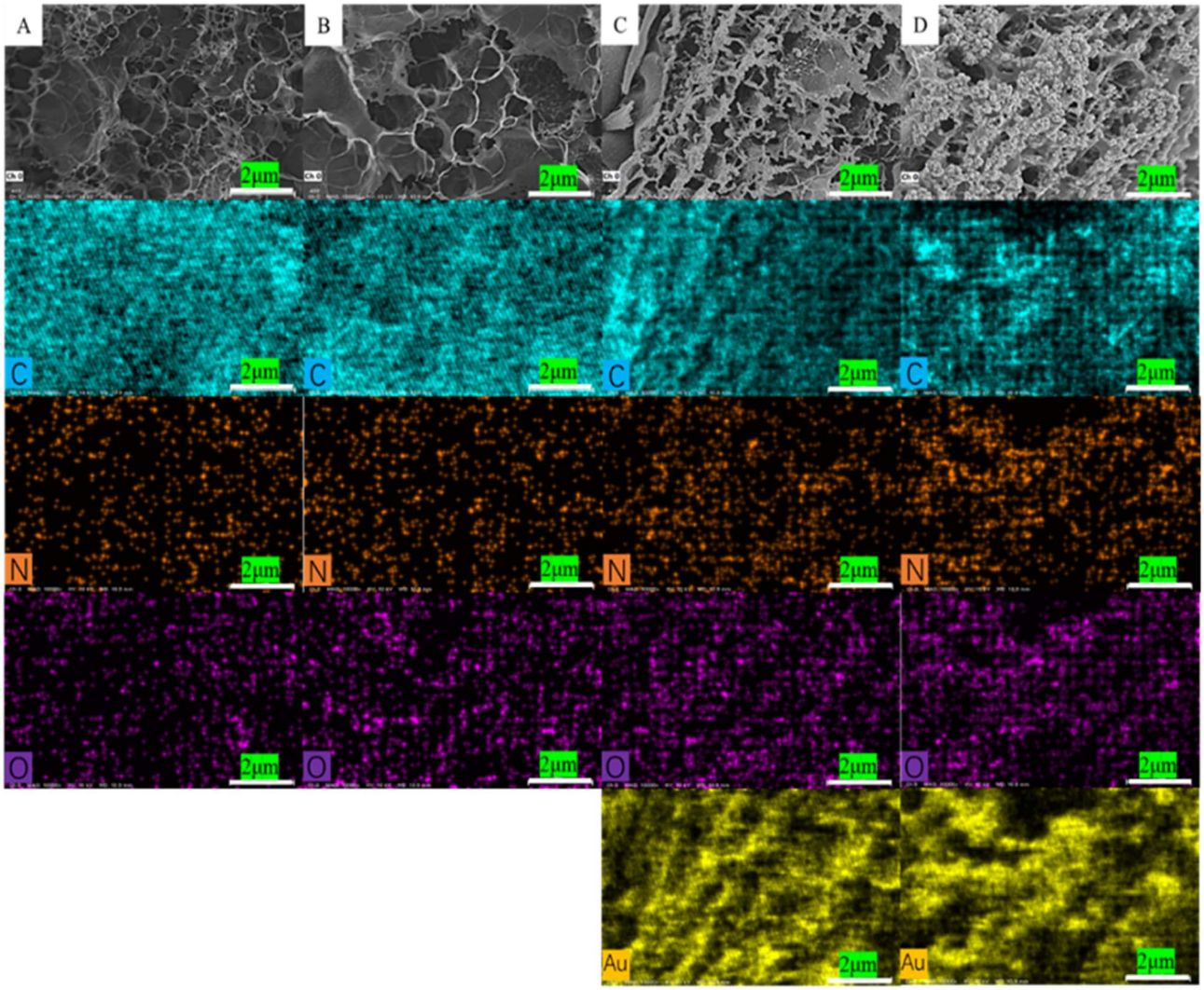

Fig. 2 EDS diagram of the element distribution on the electrode surface (A) LIG electrode, (B) LIG/PEDOT electrode, (C) LIG/PEDOT/Au electrode, (D) LIG/PEDOT/Au/GOx (BSA) electrode.

empty atmosphere, resulting in a small amount of nitrogen and oxygen elements being doped during modification. This phenomenon may lead to a decrease in electron transfer efficiency on the electrode surface. However, it can improve the hydrophilicity of the electrode surface and increase the number of active sites to some extent. Fig. 2B indicates an increase in oxygen content, which proves that the EDOT monomer polymerized on the LIG electrode surface. The dense distribution of Au element in Fig. 2C indicates that a significant number of Au NPs were successfully assembled on the LIG/PEDOT electrode surface. Furthermore, the content of oxygen elements increased with GOx modification on the modified electrode, as shown in Fig. 2D, owing to the rich oxygen content of GOx. The content of N and O elements significantly increased in Fig. 3 due to the introduction of a considerable number of groups containing N and O elements after fixing GOx, BSA, and GA on the electrode surface.

The morphology and structure of LIG, LIG/PEDOT and LIG/PEDOT/Au composites were characterized by TEM (Tecnai F30

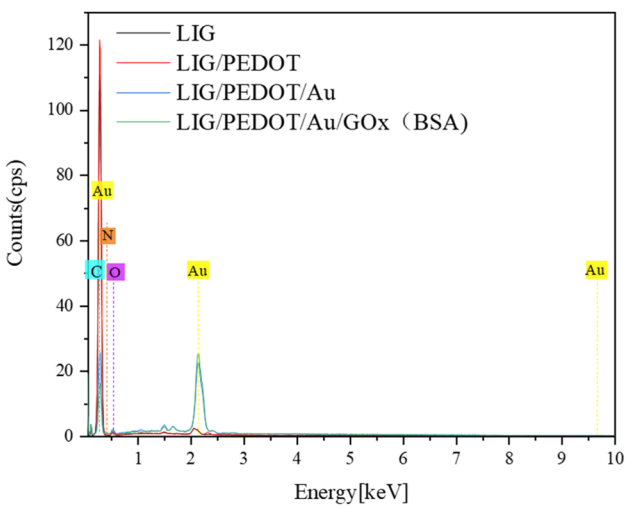

Fig. 3 EDS elemental analysis of different electrode surfaces.

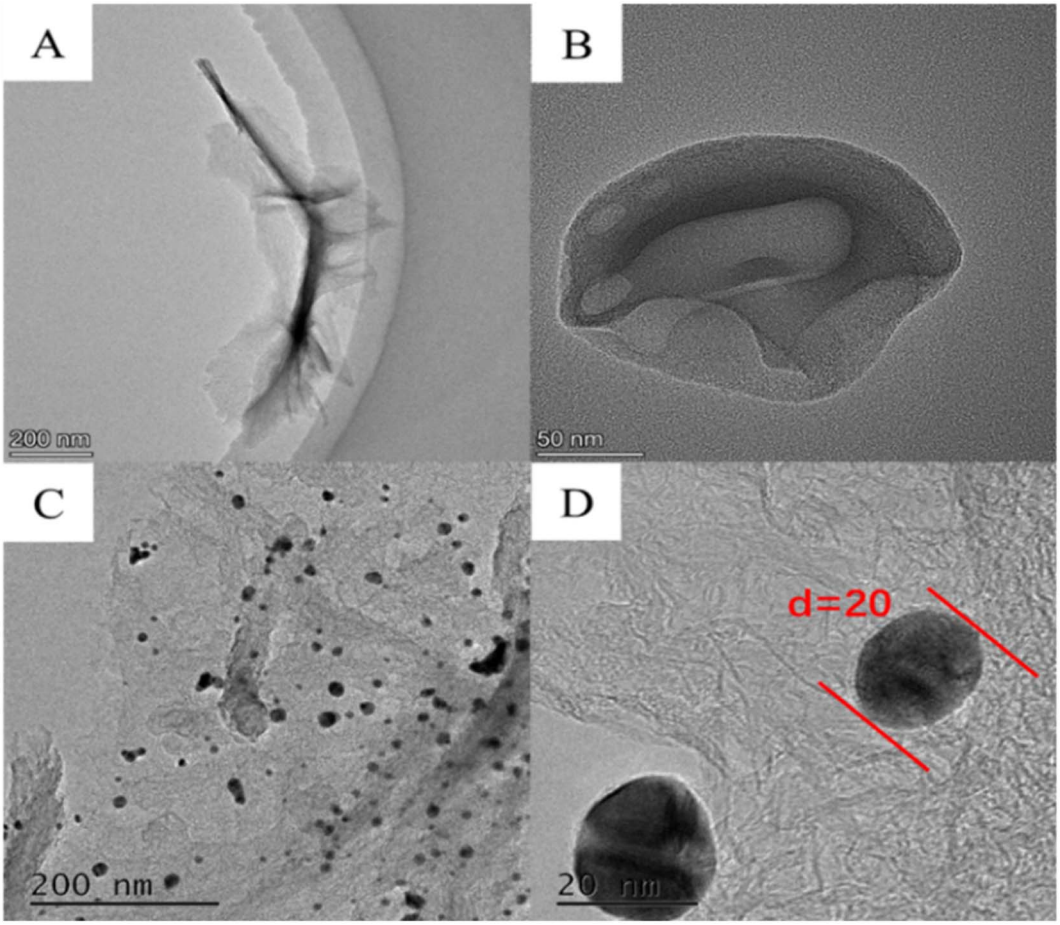

Fig. 4 TEM image of (A) LIG, (B) LIG/PEDOT, (C and D) LIG/PEDOT/Au nanomaterials.

G2 STWIN 300 kV). As illustrated in Fig. 4A, the prepared material features a distinct flake graphene structure, indicating that laser printing technology has effectively transformed PI into graphene. The surface of graphene displays translucency in both the center and edge regions, indicating that the EDOT monomer has successfully polymerized on the electrode surface through electrodeposition (Fig. 4B). Fig. 4C depicts a uniform distribution of granular material with a size of around 20 nm adhering to the electrode surface, indicating that Au NPs have been deposited onto the surface.

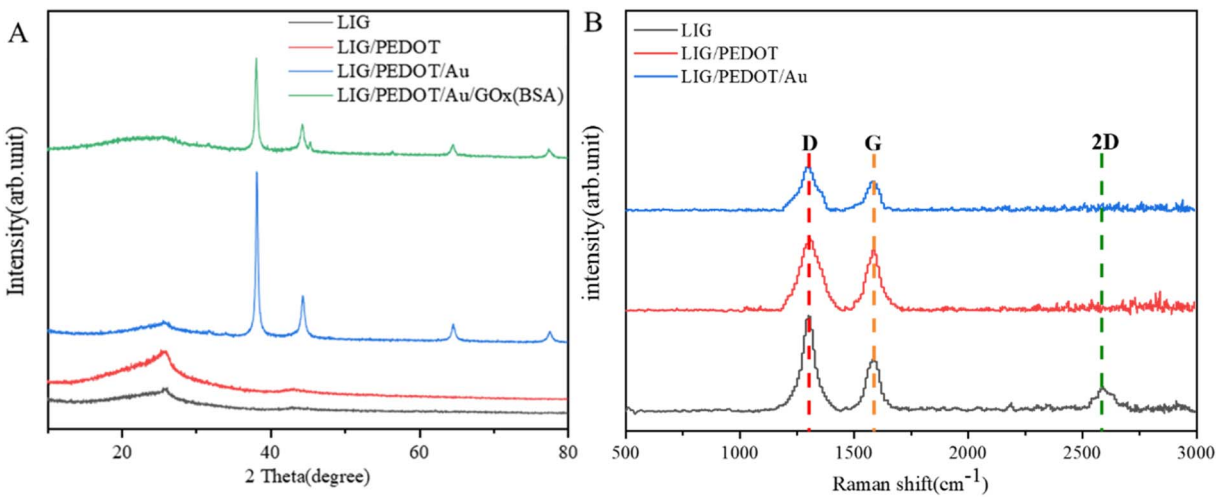

Fig. 5 (A) XRD spectra and (B) Raman spectra of LIG, LIG/PEDOT, LIG/PEDOT/Au, LIG/PEDOT/Au/GOx (BSA) composite materials.

The structure of different electrodes was characterized using X-ray diffraction (XRD, Rigaku Smart Lab, Japan). As shown in Fig. 5A, the characteristic peak of graphene at $2\theta = 25.92°$ was observed for all electrodes, indicating the successful graphitization of the PI film. While there is no obvious diffraction peak in the PEDOT polymer, thus it is not reflected in the XRD diagram. The reflection peaks of Au face-centered cubic crystal structure at 38.12°, 44.32°, 64.68°, 77.68° and 81.93° were observed for the LIG/PEDOT/Au and LIG/PEDOT/Au/GOx (BSA) electrodes, indicating that Au was successfully modified on the electrode surface.

Raman spectroscopy is a valuable non-destructive tool for investigating the properties of carbon-based compounds. Herein, Raman spectroscopy further characterizes the graphitization effect of LIG electrode materials (Fig. 5B). Three typical graphene fingerprint vibration peaks are observed, which are G band at 1580 cm^{-1}, D band at 1302 cm^{-1} and 2D band at 2594 cm^{-1}. The intensity ratio of the G peak to the 2D peak is generally accepted to correlate with the number of graphene layers. Specifically, a higher G peak height than the 2D peak height indicates a multi-layer stacked structure in laser-induced graphene. Furthermore, the Raman scattering results of the composite electrode showed that the 2D peak disappeared, which potentially due to the change in the chemical environment and surface structure of the graphene after modification of the LIG electrode material, thereby affecting the scattering efficiency of graphene.

3.3 Electrochemical activity of electrodes

The electrochemical behavior of the electrode was investigated by cyclic voltammetry in a potassium ferrocyanide solution. As shown in Fig. 6A, the LIG electrode exhibited excellent electrochemical performance and reversibility. In comparison to traditional electrodes, the LIG electrode displayed significantly higher electrochemical activity.[43] The current response of the electrode was gradually improved after depositing PEDOT and Au NPs on the surface of the LIG electrode. This is because PEDOT, as a conductive polymer, effectively improves charge transfer, while its high hydrophilicity increases the biocompatibility of the modified electrode. Additionally, Au NPs improve the effective area of the electrode, providing more enzyme immobilization sites, and promoting the electron transfer efficiency of the electrode surface. GOx was immobilized on the LIG/PEDOT/Au composite electrode through covalent cross-linking between molecules and hydrogen bonding between carboxyl and carboxyl groups. The immobilization of enzymes and proteins on the electrode surface significantly decreased the electron transfer efficiency and peak current, indicating successful modification of GOx on the electrode surface.

According to the calculation method in ref. 44, the effective area (A_{eff}) of electrode surface after modifications can be calculated according to Randles–Sevcik equation:

$$I_p = 2.69 \times 10^5 A_{eff} n^{2/3} D_0^{1/2} C_0 v^{1/2} \quad (1)$$

Here, n, D_0, C_0, I_p and v are the number of transferred electrons ($n = 1$), the diffusion coefficient of potassium ferricyanide solution (0.673×10^{-5} cm^2 s^{-1}), the volume concentration of redox probe (5×10^{-6} mol cm^{-3}), the peak current of oxidation peak and the scanning rate of electrochemical workstation (0.1 V s^{-1}), respectively. The values of A_{eff} from the LIG, LIG/PEDOT, LIG/PEDOT/Au, LIG/PEDOT/Au, LIG/PEDOT/Au/GOx electrodes are 0.418, 0.450, 0.535, 0.306 cm^2, respectively. The modification of PEDOT and Au NPs increases the effective area of the electrodes, while the surface resistance of LIG/PEDOT/Au/GOx (BSA) electrodes increases due to the modification of GOx and BSA, leading to a decrease in effective area.

After enzyme modification, the effective surface area of the electrode remained four times greater than its modified geometric area, which measures 0.07 cm^2 (assuming π to be 3.14).

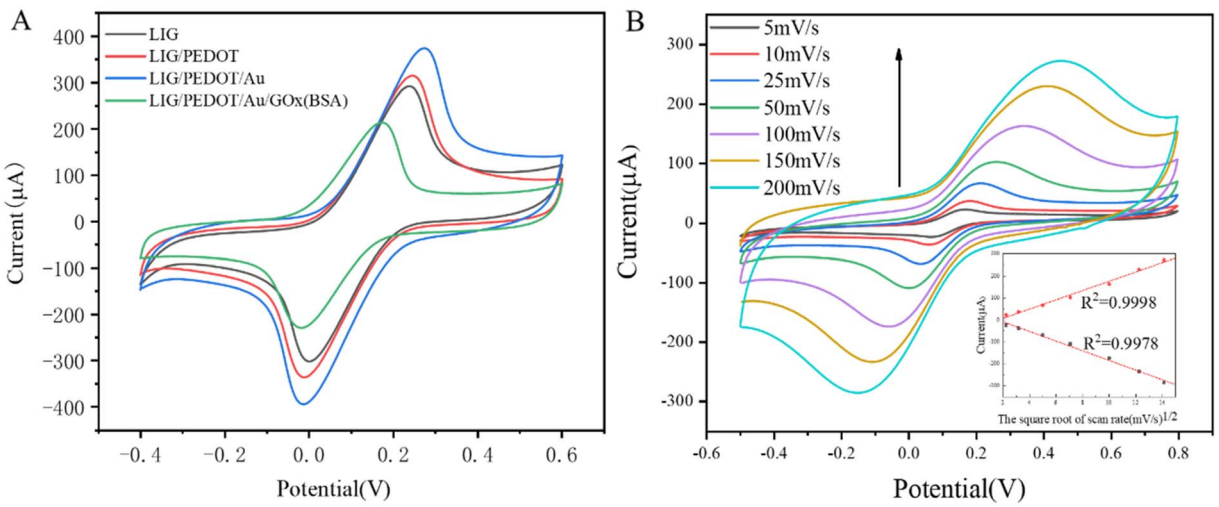

Fig. 6 (A) Cyclic voltammetric curves of different modified electrons in potassium ferricyanide solution; (B) cyclic voltammograms of LIG/PEDOT/Au/GOx (BSA) election at different scanning speeds in potassium ferricyanide solution (inset: linear relationship between peak current intensity and square root of sweet speed).

The amount of protein loaded onto the electrode surface could be calculated by Faraday formula:

$$I_p = \frac{nFQ_v}{4RT} = \frac{n^2F^2A\Gamma v}{4RT} \quad (2)$$

$$\Gamma = \frac{Q}{nFA_{eff}} \quad (3)$$

where n is the number of transferred electrons in the electrochemical reaction process, $n = 1$; Q is the integral of oxidation peak area in CV curve; F is Faraday constant (F = 96.493 C mol^{-1}); Γ is the loading amount of modifier per unit area (mol cm^{-2}). Combining with the conclusion of formula (1), the Γ values of LIG/PEDOT/Au and LIG/PEDOT/Au/GOx (BSA) surface modifiers are calculated to be 1.13×10^{-9} mol cm^{-2} and 1.57×10^{-9} mol cm^{-2}, respectively. Therefore, the number of biomolecules immobilized on the electrode surface per unit area is 4.4×10^{-10} mol cm^{-2}.

Fig. 6B shows the cyclic voltammetry curves of LIG/PEDOT/Au/GOx (BSA) electrode in the presence of $K_3[Fe(CN)_6]$ redox medium solution at different sweeping rates. The inset figure of

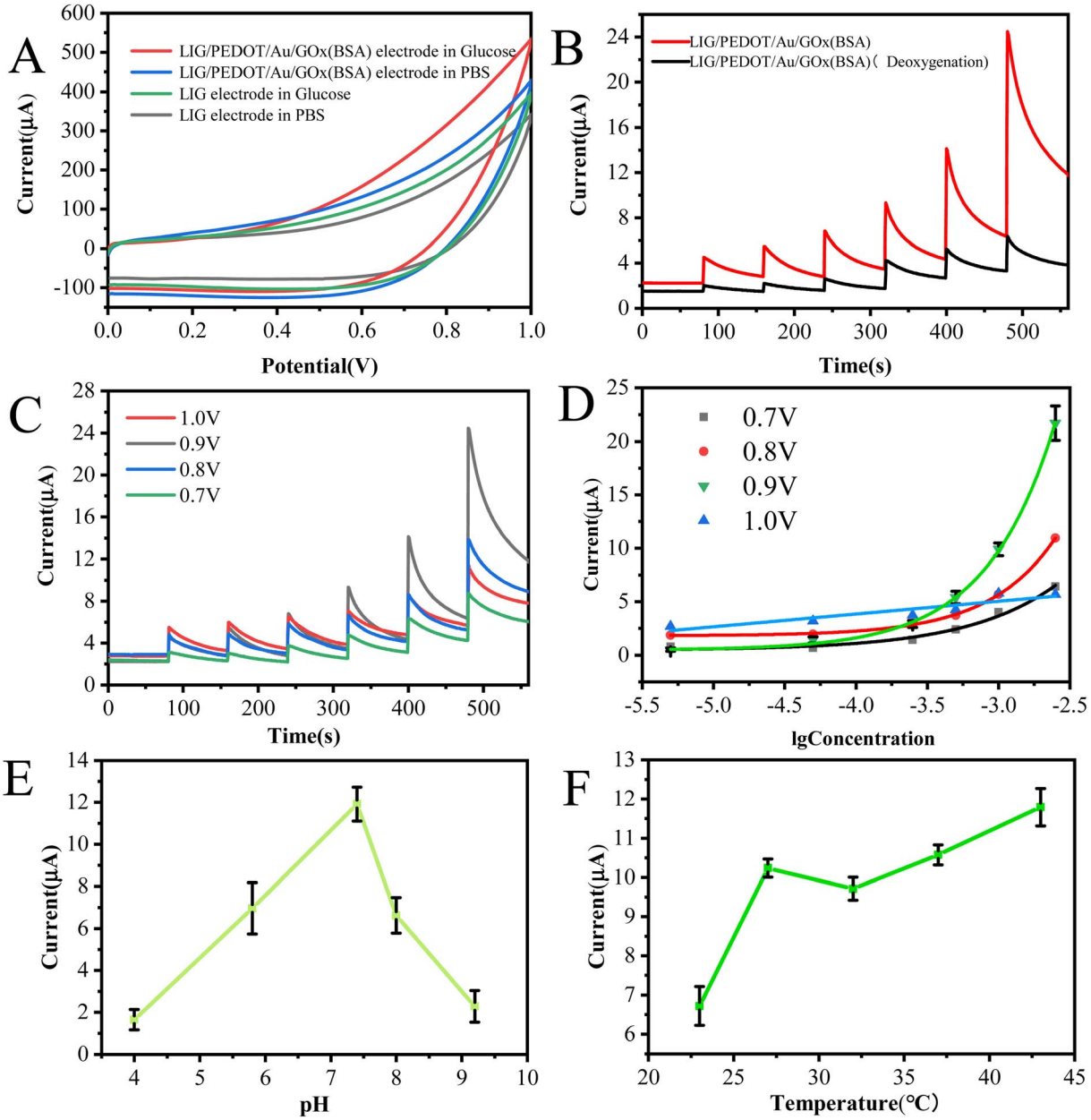

Fig. 7 Cyclic voltammograms of LIG, LIG/PEDOT/Au/GOx (BSA) electrodes in PBS and glucose solutions (A); i–t curves of LIG/PEDOT/Au/GOx (BSA) electrode for glucose sensor under both aerobic and anaerobic conditions (B); i–t curves (C) and fitting curves (D) of LIG/PEDOT/Au/GOx (BSA) electrode for glucose sensor at different potentials; variation curves of glucose sensors at different pH (4.0, 5.8, 7.4, 7.8 and 9.1) (E) and temperature (23, 27, 32, 37 and 42 °C) (F). The scanning rate is 0.1 V s^{-1} (A); the concentration of glucose solution from left to right is: 0.5×10^{-5}, 0.5×10^{-4}, 2.5×10^{-4}, 5.0×10^{-4}, 1.0×10^{-3}, 2.5×10^{-3} mol L^{-1} (B and C); glucose solution concentration is 1.0×10^{-3} mol L^{-1} (E and F).

Fig. 6B illustrates that both anodic and cathodic peak currents increased proportional with the increasing $\nu^{1/2}$ (ν is sweep rate) in the examined range of 5 to 200 mV s^{-1}, which indicate that the surface reaction of LIG/PEDOT/Au/GOx (BSA) electrode is a typical diffusion-controlled reaction. The inset figure of Fig. 6B illustrates that both anodic and cathodic peak currents increased proportional with the increasing $\nu^{1/2}$ (ν is sweep rate) in the examined range of 5 to 200 mV s^{-1}, which indicate that the surface reaction of LIG/PEDOT/Au/GOx (BSA) electrode is a typical diffusion-controlled reaction.

3.4 Effects of different conditions on the electrochemical activity of electrodes

The catalytic effect of different electrodes on glucose solution were investigated using cyclic voltammetry. As shown in Fig. 7A, the electrochemical response of LIG electrode and LIG/PEDOT/Au/GOx (BSA) electrode in glucose solution is higher than that in PBS solution, indicating the catalytic effect of both electrodes on glucose. However, the GOx-modified electrode showed the highest current response because the glucose solution was catalyzed by GOx, indicating the effective enzymatic catalytic activity of the GOx modified on the LIG/PEDOT/Au electrode. And it also reflects that LIG/PEDOT/Au electrode provides a biocompatible microenvironment to maintain the native structure of the immobilized GOx.

The catalytic activity of GOx towards glucose is significantly influenced by the presence of dissolved oxygen. The deoxidization experiment of LIG/PEDOT/Au/GOx (BSA) glucose sensor electrode was carried out to explore the influence of O_2 on the performance of glucose sensor. The catalytic reaction process can be expressed by the following formula:[1]

$$\text{GOx (FAD)} + \text{glucose} \rightarrow \text{GOx (FADH}_2\text{)} + \text{gluconolactone} \quad (4)$$

$$\text{GOx (FADH}_2\text{)} + \text{O}_2 \rightarrow \text{GOx (FAD)} + \text{H}_2\text{O}_2 \quad (5)$$

$$\text{GOx (FADH}_2\text{)} \rightleftharpoons \text{GOx (FAD)} + 2e + 2\text{H}^+ \quad (6)$$

Flavin adenine dinucleotide (FAD) is an essential component of the GOx molecule that undergoes a redox reaction. Specifically, GOx (FAD) oxidizes glucose to gluconolactone acid, while the reduced GOx ($FADH_2$) reduces O_2 to H_2O_2 in the presence of O_2. Direct electron transfer between GOx and the electrode surface results in an electrochemical response.[39] Under nitrogen deoxidization conditions, GOx (FAD) is reduced to GOx ($FADH_2$), but H_2O_2 production is inhibited, leading to only a limited electron transfer. As shown in Fig. 7B, the LIG/PEDOT/Au/GOx electrode generated a current signal that increased with the concentration of glucose solution in the absence of deoxidization. While under deoxygenation conditions, the current signal does not change significantly even with increasing glucose concentration. Therefore, efficient and stable glucose catalysis with GOx requires careful control of the dissolved oxygen level in the reaction environment.

The effect of potential value on chronoamperometry is to regulate the rate and direction of electrochemical reactions. Adjusting the potential value can control reaction rate and selectivity, ultimately influencing the changes in current. In order to enhance the electrochemical performance of the prepared electrode, we compared the i–t curves of glucose solutions with varying concentrations measured at different potentials. Analysis of the i–t curves in Fig. 7C reveals noticeable differences in current response under different constant potentials. The current response increases with an increase in potential until it reaches optimal response at a constant potential of 0.9 V. However, further increase of potential to 1.0 V results in a decrease of current response. It can be concluded that although high potential is beneficial for generating high current response, excessive potential may activate interfering substances and produce many intermediates, leading to irreversible reactions and inhibition of glucose oxidation. Therefore, the LIG/PEDOT/Au/GOx (BSA) electrode produces the best catalytic effect on glucose at a potential of 0.9 V.

To investigate the impact of glucose sensing in various pH and temperature environments, we conducted chronoamperometry experiments on glucose catalysis using LIG/PEDOT/Au/GOx electrodes in different detection environments. Fig. 7E shows that at pH 7.4, the LIG/PEDOT/Au/GOx (BSA) electrode exhibited the highest response to the current generated by electrochemical enzyme catalysis of glucose solution. It is well known that GOx enzyme activity is reduced in alkaline environments and enhanced in acidic environments. This is due to the conformational changes in the enzyme molecules caused by the acidic or alkaline environment, which affect GOx's ability to bind to glucose. Therefore, to maintain the optimal enzyme activity and stability of glucose oxidase, it is usually necessary to perform reactions or preservation in a neutral or slightly acidic environment. In addition, the activity of enzymes and the electrical properties of liquids are influenced by temperature. To ensure the reliability of measurement data, the influence of temperature on sensor performance should be tested (Fig. 7F). The results indicate that the enzyme activity of the electrochemical sensor may be inhibited at an ambient temperature of 23 °C, but the sensor can still maintain a high response current over a wide temperature range. Therefore, pH and temperature have an impact on the performance and practical application of enzyme electrodes. In practical applications, it is necessary to regulate the pH value with neutral buffer solutions and control the ambient temperature within the range of 27 to 37 °C. When a sensor is simultaneously affected by the pH and temperature, it can be addressed by employing a multimodal sensing decoupling mechanism. Each sensing modality can be calibrated and optimized independently to eliminate the cross-interference between pH and temperature.[45,46] Calibration can be performed to establish the correlation between the output of each sensing modality of the pH and temperature, enabling the creation of suitable calibration curves or algorithms. By integrating the data from multiple sensing modalities, accurate measurements of the pH and temperature of the solution can be obtained. Through decoupling the sensing mechanisms, each modality can work independently without being influenced by other modalities, enhancing the accuracy and reliability of the sensor. In the current study, working curves can be created in different pH

solution by fixing the temperature and in different temperature by fixing pH to perform calibration.

3.5 Working curves

Glucose solutions with various concentrations were measured under the optimized experimental conditions to establish working curves. The obtained *i–t* curves are shown in Fig. 8A. Compared with bare LIG electrode and LIG/PEDOT/Au/MUA composite electrode, the LIG/PEDOT/Au/GOx (BSA) composite electrode showed a more sensitive current response to glucose solution, which indicates that GOx plays a key role in the electrocatalytic oxidation of glucose.

Draw a working curve between the chronocurrent values obtained at different concentrations and the logarithm of glucose concentration. It can be observed that the current response of LIG/PEDOT/Au/GOx (BSA) electrode increases exponentially with the logarithm of glucose solution concentration from 0.5×10^{-5} mol L^{-1} to 2.5×10^{-3} mol L^{-1}, with an excellent sensitivity of 341.67 μA mM^{-1} cm^{-2} and an ultra-low limit of detection (S/N = 3) of 0.2×10^{-5} mol L^{-1}. While the current response of the electrode without GOx modification remains unchanged with the increase of glucose solution concentration (Fig. 8B). Compared with commercial conventional glucose meter (Counter Plus 7600P), the present sensor has a higher sensitivity and wider detection range (Table 1). In order to further evaluate the glucose detection performance of the electrode, the comparison of electrochemical sensors for glucose detection based on enzymatic and non-enzymatic sensors was listed in Table 2. From Table 2, it can be seen that non-enzymatic sensors exhibit higher sensitivity due to the excellent catalytic performance and conductivity of nanoenzymes, and often displayed weak competitiveness in complex matrices due to less specificity of nanoenzymes than biological enzymes. Electrochemical glucose sensors based on LIG combined with nanoenzymes, exhibit ultra-high sensitivity.[24,39] The non-enzymatic sensors and the present enzyme sensor both use patternable flexible LIG electrodes, promoting the development of LIG technology from a single detection component to an integrated intelligent detection system. The continuous semiconductor laser with 450 nm wavelength in this study has a lower cost and is environmentally friendly. Moreover, the mesoporous structure of LIG electrode improves the electrochemical response, and is conducive to electrode modification. The modification of Au and PEDOT on LIG electrode effectively enhances the sensitivity of glucose oxidase sensor. Furthermore, PEDOT can protect LIG mesoporous structure and have excellent anti fouling ability, making the modified electrode more stable and capable of analyzing actual samples. Research shows that it does not require a special solution environment and can analyze samples in pH and temperature environments of human sweat, urine, and blood samples, avoiding unnecessary measurement steps. In addition, the sensor shows excellent portable for real-time detection combined with smartphone.

3.6 Performance of the glucose sensor

After the modified enzyme receptor, the electrode gains specific recognition ability for a particular biological molecule. To investigate the selectivity of the LIG/PEDOT/Au/GOx electrode for glucose sensing, several interfering substances, including urea, NaCl, tartaric acid, sucrose, galactose, and lactosyl acid

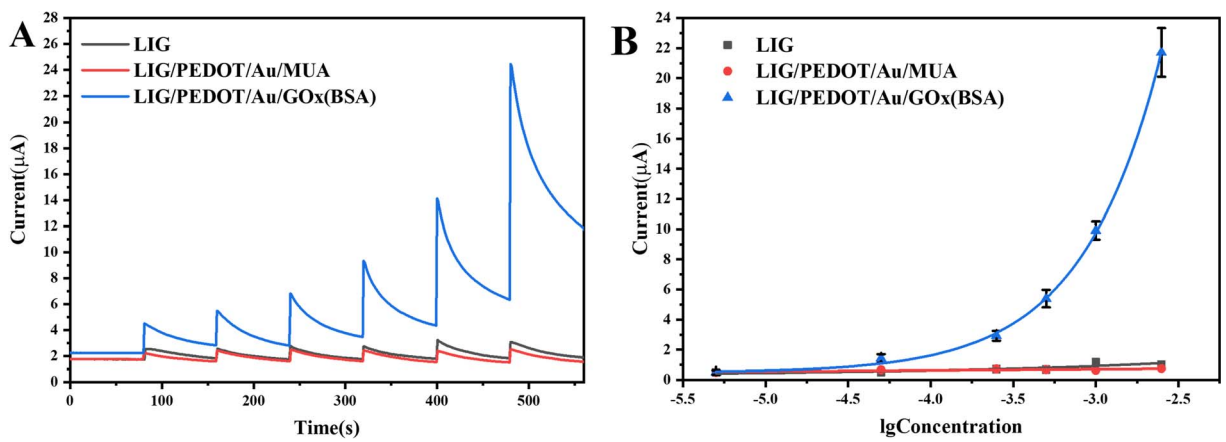

Fig. 8 *i–t* curves (A) and working curves (B) of LIG, LIG/PEDOT/Au/MUA, LIG/PEDOT/Au/GOx (BSA) electrodes against glucose solution; the gradient concentrations of glucose solution were 0.5×10^{-5}, 0.5×10^{-4}, 2.5×10^{-4}, 5.0×10^{-4}, 1.0×10^{-3}, 2.5×10^{-3} mol L^{-1}.

Table 1 The comparison of commercial glucose meter for glucose detection

Methods	Dynamic ranges/(mmol L^{-1})	Working curve equations	Correlation coefficients	LOQ/(mmol L^{-1})
Blood glucose meter	0.6–33.3	$y = 5.42x + 0.65$	0.9453	0.6
The present method	0.005–2.5	$y = 4875.48 \times \exp(x/0.48) + 0.48$	0.9932	0.002

Table 2 The comparison of electrochemical sensors for glucose detection[a]

Electrode	Recognition elements	Detection methods	Sensitivity ($\mu A\ mM^{-1}\ cm^{-2}$)	LOD (μM)	Linear range	Measurement environment	Operating voltage (V)	Characteristics	Ref.
Cu_2O/PEDOT/RGO/GCE	Cu_2O	Chronoamperometry	4700.00	0.14	0.004–3.2 mM	0.1 M NaOH	0.55	The response time was only 0.9 s, which had good stability and selectivity. No actual sample analysis was conducted	47
LSGE/AuNPs	AuNPs	Linear sweep voltammetry	0.044 ± 0.005 mA/log(M)	6.30	10 μM–10 mM	0.5 M KOH	No	The electrode preparation method is simple, low-cost, and has good selectivity. No stability and actual sample analysis was done	48
Ni/Au/LIG	Ni	Chronoamperometry	3500.00	1.50	0–1 mM	0.05 M NaOH	0.5	The requirement for solution environment is relatively low, and the porous encapsulation reaction chamber can better collect sweat. Has good selectivity, but has not undergone stability analysis	49
AgNRs/AuNPs–GO–CNT/LIG	Ag/AuNPs	Chronoamperometry	1317.69	0.08	0.1–5 mM	0.1 M NaOH	0.7	The porous graphene sensor modified with nanocomposites has good selectivity, can also detect pH value, and exhibits extraordinary stability, maintaining sensitivity of over 91% under environmental conditions for 21 days	32
GOx/FCA/PEG/SWCNT	GOx	Chronoamperometry	5.50	28.00	0–10 mM	PBS (pH 7.4)	0.3	A simple electrochemical sensing platform based on single walled carbon nanotube (SWCNT) electrodes has good selectivity and stability. No actual sample analysis was conducted	1
GOx/LIG	GOx	Chronoamperometry	43.15	431.00	0.431–8 mM	PBS (pH 7.0)	0.8	Simple preparation, low cost, and reliable stability. Has good selectivity and stability, but has not undergone actual sample analysis. The detection limit is high, and sensing needs further optimization	50
GOx/$Ti_3C_2T_x$ MXene	GOx	Cyclic voltammetry	93.75	12.10	0.1–10 mM	PBS (pH 7.0)	No	A glucose data collection and sharing system based on cloud platform is developed, but the detection limit is high. Has good selectivity and stability, but has not undergone actual sample analysis	51

Table 2 (*Contd.*)

Electrode	Recognition elements	Detection methods	Sensitivity ($\mu A\ mM^{-1}\ cm^{-2}$)	LOD (μM)	Linear range	Measurement environment	Operating voltage (V)	Characteristics	Ref.
GCE–RFG–RGO–GOD–CS	GOD	Chronoamperometry	46.71	79.65	0.08–3 mM	PBS (pH 7.0)	−0.5	It had good sensitivity with a relative standard deviation (RSD) of 4.49%. But has not undergone selectivity and actual sample analysis	52
GOx/Au/PEDOT/LIG	GOx	Chronoamperometry	341.67	2.00	0.005–2.5 mM	PBS (pH 7.4)	0.9	The continuous semiconductor laser with 450 nm wavelength has a lower cost and is environmentally friendly. The 3D mesoporous LIG electrode materials, combined with Au and PEDOT modification endows the sensor with excellent sensitivity, stability, and anti-fouling ability. The flexibility and simple method, combined with smart phones are expected to achieve portable real-time detection. It has good application prospect in analysis of actual samples, such as blood, sweat, and urine	This work

[a] RGO (reduced graphene oxide); GCE (glassy carbon electrode); FCA (ferrocenecarboxylic acid); PEG (polyethylene glycol); SWCNT (single-walled carbon nanotubes); LSGE (laser-scribed graphene electrode); RFG (reduced functionalized graphene); CS (chitosan); PB (Prussian blue); NC (nanocomposite); SPCE (screen-printed electrode); GOD (glucose oxidase).

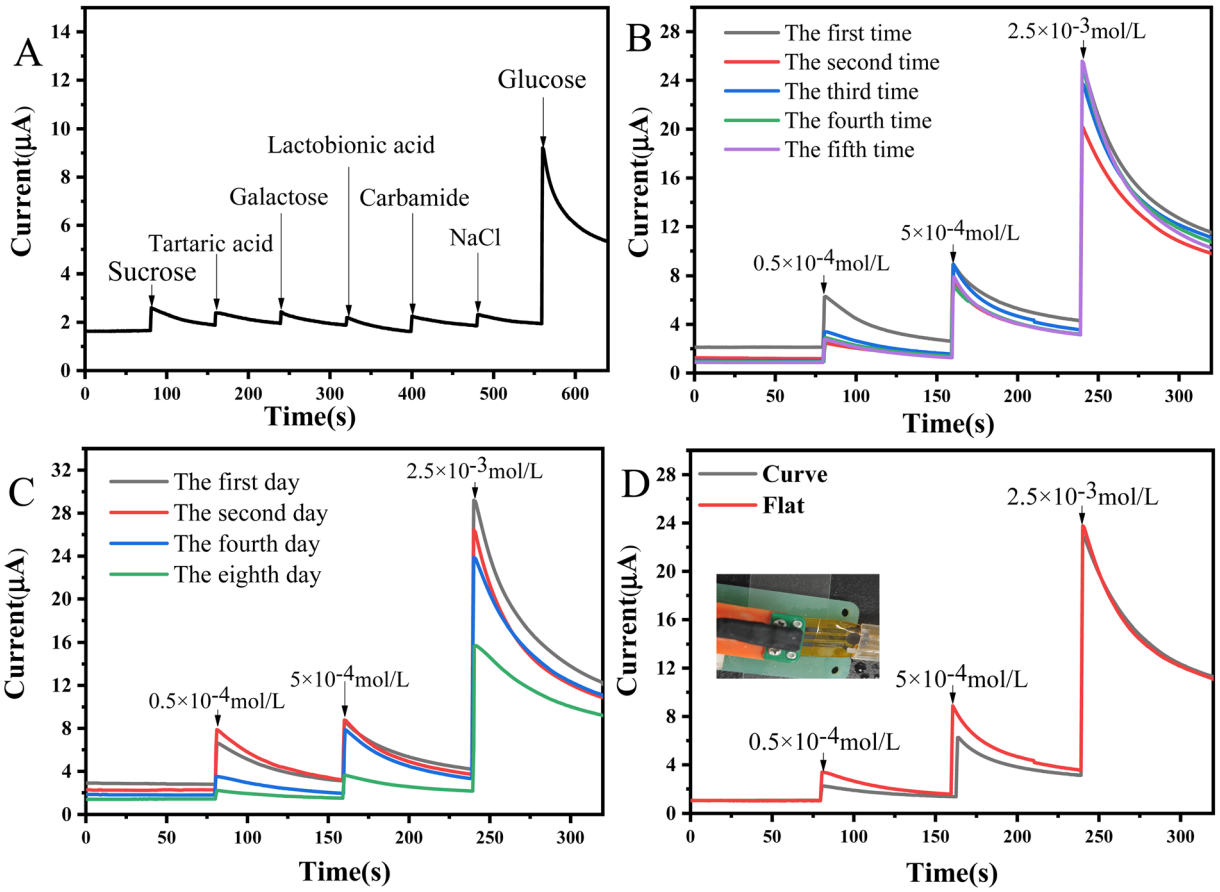

Fig. 9 *i*–*t* curves of LIG/PEDOT/Au/GOx (BSA) electrode for selectivity (A), reusability (B), stability (C); *i*–*t* curves of flexible LIG/PEDOT/Au/GOx (BSA) electrode under different bending states (D).

were selected for analysis *via* chronoamperometry. The results of the analysis, as presented in Fig. 9A, show that the interferers generated only weak current responses in comparison to glucose solutions, which indicates the high selectivity of the LIG/PEDOT/Au/GOx glucose sensing electrode. Reasonable reusability is a crucial factor for enhancing the cost-effectiveness and potential applications of a sensor. In this study, we evaluated the reusability of the LIG/PEDOT/Au/GOx electrode by repeating its use. As shown in Fig. 9B, the current signal remained largely unchanged even after five times

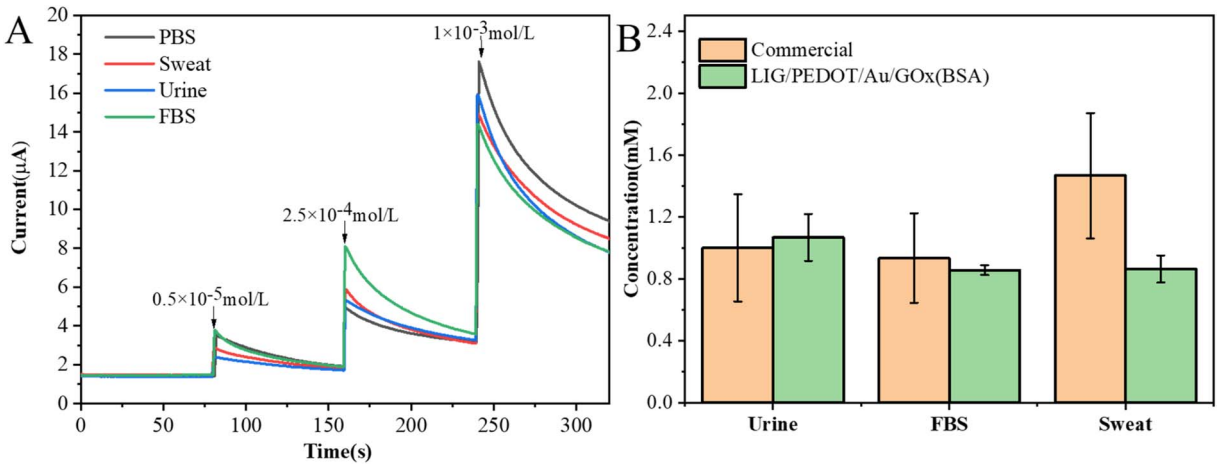

Fig. 10 (A) *i*–*t* curves of actual samples with different concentrations of glucose; (B) comparison of the measured glucose in actual samples between the commercial and our LIG-based flexible glucose sensors.

Table 3 Addition recovery rates in different biological samples

Sample	Additive concentration (mmol L^{-1})	Current (μA)	Recovery rate (%)
Urine	0	1.30	—
	0.005	2.49	61.34
	0.25	5.24	111.93
	1.0	15.91	90.52
FBS	0	1.49	—
	0.005	3.64	112.37
	0.25	7.08	159.66
	1.0	14.65	81.72
Sweat	0	1.49	—
	0.005	2.90	72.68
	0.25	5.89	125.00
	1.0	14.96	83.46
PBS	0	1.46	—
	0.005	3.40	—
	0.25	4.98	—
	1.0	17.60	—

reuse, demonstrating the electrode's excellent reusability and ability to maintain a stable current response. Furthermore, the long-term stability of the LIG/PEDOT/Au/GOx electrode was evaluated by chronoamperometry. As shown in Fig. 9C, the decrease in the electrode's current response over time may be attributed to the declining enzyme activity. Moreover, environmental factors such as temperature and humidity can also affect the electrode's electrochemical performance. Despite these influences, the electrode maintained a high current response after 8 days of storage, demonstrating its durability and efficacy over a specific time frame.

3.7 Flexibility of the LIG/PEDOT/Au/GOx electrode

PET, as a flexible substrate material, has good mechanical properties. In this study, we evaluated the electrochemical stability of LIG/PEDOT/Au/GOx electrode under internal bending conditions by simulating the bending of the electrode under external force. The results, as depicted in Fig. 9D, showed the catalytic effect on glucose in both tiled and incurved states using chronoamperometry. The *i–t* curves indicated that the current response of the electrode was consistent in both flat and bent states, demonstrating the excellent stability of LIG/PEDOT/Au/GOx electrodes under different stress conditions.

3.8 Analysis of biofluid samples

The LIG/PEDOT/Au/GOx electrode was used to analyze biological samples in order to validate the application of the glucose sensor prepared in this study. Sweat, urine and serum were selected as the base solution, and glucose solutions with low, medium and high concentrations were added respectively. The interference degree of background solution was investigated by *i–t* curves. As shown in Fig. 10A, different biological fluid samples may interfere with electron transfer on the electrode surface, but they all show good current response. The recoveries of glucose with different concentrations in urine, FBS and sweat are 61.34–111.93%, 81.72–159.66% and 72.68–125.00% respectively (Table 3). The recovery rates of urine and sweat at low

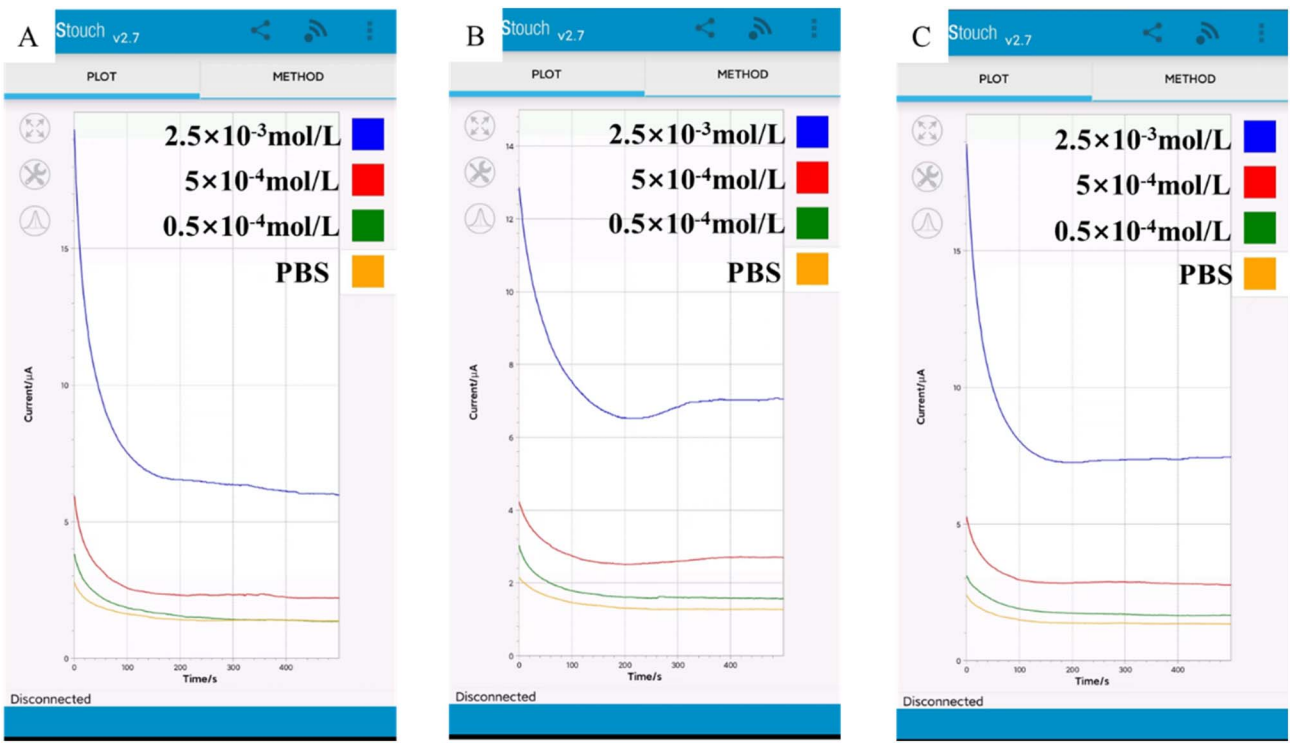

Fig. 11 SenSit Smart U disk detection device connected to Android smartphone detects (A) FBS, (B) sweat and (C) urine containing different concentrations of glucose.

glucose concentration may be more susceptible to protein salt and other components which affect the sensitivity of the electrode. The actual samples at medium and high concentrations have achieved higher recovery rates. The prepared electrodes show good step responses, which indicates that the electrodes have good sensitivity and selectivity in actual samples.

In this work, the displayed sensor has good anti-interference performance, enabling it to accurately measure glucose concentration in complex samples. In order to further verify the reliability of the sensor in actual sample detection, commercial blood glucose meters and LIG/PEDOT/Au/GOx (BSA) electrodes were used to detect actual samples containing 1 mM glucose. As shown in Fig. 10B, the results showed that for actual samples containing interfering components, commercial blood glucose meters showed significant errors, while glucose sensing electrodes showed more stable and reliable measurement values. In all, due to the low cost and portability, blood glucose meters, as commercial products, have developed maturely and are widely accepted by consumers. Compared with commercial conventional glucose meter, apart from high sensitivity and wide detection range, the present sensor has higher precision and reusability. Both of them can accurately detect complex matrix samples. But blood glucose meters are not friendly to sweat detection, which may be because the complex electrolytes in sweat interfere with glucose detection. These highlights of the present sensor, as a reliable tool for glucose monitoring, has good application prospect in challenging environments. More efforts should be made in device preparation and intelligent detection.

3.9 Smartphone detection

At present, the combination of various biosensors and intelligent devices has become a hot research direction.[53–55] The prepared LIG/PEDOT/Au/GOx electrode can be used for portable detection by connecting SenSit Smart U disk portable electrochemical analyzer combined with smart phone detection (Fig. 11). Through smart phone detection, it can be seen that the current response increases with the increase of glucose concentration, which indicates that the glucose sensing electrode can be used to detect glucose in FBS (A), sweat (B) and urine (C) by connecting smart devices. This novel approach enables the development of portable applications in conjunction with smart devices.

4 Conclusions

In conclusion, we have successfully developed a novel enzyme electrochemical sensor for glucose detection based on LIG/PEDOT/Au/GOx electrode. The experimental results indicate that the prepared portable sensor was capable of detecting glucose, showing high sensitivity, selectivity, precision and stability. More importantly, combined with smart phone detection, glucose molecules in biological fluid samples such as urine, sweat and serum can be monitored in real time. The development of this sensor provides a new idea and method for portable detection of glucose. With a simple fabrication process and many benefiting characteristics, LIG/PEDOT/Au electrode has great potential for the development of other high-performance bio electrocatalytic systems. In the future, we will further improve the performance of the sensor and explore its application in a wider range of fields to promote the development of sensor technology.

Conflicts of interest

There are no conflicts to declare.

Acknowledgements

This project was financially supported by Fujian Province Natural Science Foundation (2020J01835, 2022J011114, 2021J05203, 2021J011018), the Open Project of Fujian Key Laboratory of Functional Marine Sensing Materials, Minjiang University (MJUKF-FMSM202206), and the Natural Science Foundation of Shandong Province (ZR2021MH146).

References

1 D. K. Han, C. A. Li, S. H. Song, K. Cho, J. S. Choi, S. E. Son and G. H. Seong, *J. Anal. Sci. Technol.*, 2023, **14**, 9.
2 Y. T. Du, X. Y. Zhang, P. Liu, D. G. Yu and R. L. Ge, *Front. Chem.*, 2022, **10**, 94428.
3 W. V. Gonzales, A. T. Mobashsher and A. Abbosh, *Sensors*, 2019, **19**, 800.
4 K. S. Rizi, *Curr. Opin. Electrochem.*, 2022, **32**, 100925.
5 Z. P. Zhou, T. Shu, Y. F. Sun, H. X. Si, P. W. Peng, L. Su and X. J. Zhang, *Biosens. Bioelectron.*, 2021, **192**, 113530.
6 J. L. Liu, H. J. Ji, X. Y. Lv, C. J. Zeng, H. M. Li, F. G. Li, B. Qu, F. Y. Cui and Q. Zhou, *Microchim. Acta*, 2022, **189**, 54.
7 Y. D. Xu, Q. H. Fei, M. Page, G. G. Zhao, Y. Ling, D. Chen and Z. Yan, *Nano Res.*, 2021, **14**, 3033–3050.
8 L. B. Huang, J. J. Su, Y. Song and R. Q. Ye, *Nano-Micro Lett.*, 2020, **12**, 157.
9 H. Yoon, J. Nah, H. Kim, S. Ko, M. Sharifuzzaman, S. C. Barman, X. Xuan, J. Kim and J. Y. Park, *Sens. Actuators, B*, 2020, **311**, 127866.
10 B. L. Zhang, X. Jin, L. H. Sun and X. D. Guo, *Microchem. J.*, 2020, **158**, 105217.
11 T. Naik, S. Saravanan, K. N. S. Saravana, U. Pratiush and P. C. Ramamurthy, *Mater. Chem. Phys.*, 2020, **245**, 122798.
12 E. L. Brightbill, K. T. Young, H. F. Gezahagne, D. S. Jin, B. Hitchcock and E. M. Vogel, *2D Mater.*, 2021, **8**, 025015.
13 B. X. Xu, Y. P. Hu, Q. X. Shu, M. Wang, Z. Y. Chen, W. Wei, J. M. Wen, R. Li, F. S. Liao, L. Cheng and H. Fan, *J. Chin. Chem. Soc.*, 2022, **69**, 822–830.
14 B. Zhao, Y. W. Zhou, J. F. Qu, F. Yin, S. Q. Yin, Y. W. Chang and W. Zhang, *Sens. Rev.*, 2022, **42**, 544–553.
15 S. Zhang, M. Sharifuzzamn, S. M. S. Rana, M. Abu Zahed, S. Sharma, Y. Shin, H. Song and J. Y. Park, *Nano Res.*, 2023, **16**, 7627–7637.
16 L. Meng, A. P. F. Turner and W. C. Mak, *ACS Appl. Mater. Interfaces*, 2021, **13**, 54456–54465.

17 M. Abu Zahed, S. C. Barman, P. S. Das, M. Sharifuzzaman, H. S. Yoon, S. H. Yoon and J. Y. Park, *Biosens. Bioelectron.*, 2020, **160**, 112220.
18 S. Fu, G. L. Fan, L. Yang and F. Li, *Electrochim. Acta*, 2015, **152**, 146–154.
19 Y. Zhao, Q. Zhai, D. Dong, T. An, S. Gong, Q. Shi and W. Cheng, *Anal. Chem.*, 2019, **91**, 6569–6576.
20 P. Zhihua, Z. Xingguo, Y. Haixia, T. Jiaan, C. Hailong, L. Yuncong, S. Xiao, W. Ridong, Z. Lei and L. Dachao, *Sci. Adv.*, 2021, **7**, eabd0199.
21 C. Zhang, H. Chen, X. Ding, F. Lorestani, C. Huang, B. Zhang, B. Zheng, J. Wang, H. Cheng and Y. Xu, *Applied Physics Reviews*, 2022, **9**, 011413.
22 Y. Yu, J. Nassar, C. Xu, J. Min, Y. Yang, A. Dai, R. Doshi, A. Huang, Y. Song, R. Gehlhar, A. D. Ames and W. Gao, *Sci. Robot.*, 2020, **5**, eaaz7946.
23 L. Li, J. Meng, X. Bao, Y. Huang, X.-P. Yan, H.-L. Qian, C. Zhang and T. Liu, *Adv. Energy Mater.*, 2023, **13**, 2203683.
24 M. Parrilla, A. Vanhooydonck, M. Johns, R. Watts and K. De Wael, *Sens. Actuators, B*, 2023, **378**, 133159.
25 Y. Ren, F. Meng, S. Zhang, B. Ping, H. Li, B. Yin and T. Ma, *Carbon Energy*, 2022, **4**, 446–457.
26 Y. Yang, C. Lu, L. Shen, Z. Zhao, S. Peng and C. Shuai, *J. Magnesium Alloys*, 2023, **11**, 629–640.
27 S. F. Shaikh, N. El-Atab, M. M. Hussain and I. C. Soc, *2021 IEEE 71st Electronic Components and Technology Conference (ECTC)*, 2021, pp. 2189–2195.
28 N. Yi, Y. Gao, A. Lo Verso, J. Zhu, D. Erdely, C. Xue, R. Lavelle and H. Cheng, *Mater. Today*, 2021, **50**, 24–34.
29 S. Zhang, W. Zhao, J. Zeng, Z. He, X. Wang, Z. Zhu, R. Hu, C. Liu and Q. Wang, *Mater. Today Bio*, 2023, **20**, 100638.
30 J. Zhu, S. Liu, Z. Hu, X. Zhang, N. Yi, K. Tang, M. G. Dexheimer, X. Lian, Q. Wang, J. Yang, J. Gray and H. Cheng, *Biosens. Bioelectron.*, 2021, **193**, 113606.
31 Y. Cheng, X. Gong, J. Yang, G. Zheng, Y. Zheng, Y. Li, Y. Xu, G. Nie, X. Xie, M. Chen, C. Yi and L. Jiang, *Biosens. Bioelectron.*, 2022, **203**, 114026.
32 F. Lorestani, X. Zhang, A. M. Abdullah, X. Xin, Y. Liu, M. M. Rahman, M. A. S. Biswas, B. Li, A. Dutta, Z. Niu, S. Das, S. Barai, K. Wang and H. Cheng, *Adv. Funct. Mater.*, 2023, 2306117.
33 H. R. Liang, H. X. Ma, X. R. Duan, J. Yu, H. M. Wang, S. Li, M. J. Zhu, A. B. Chen, H. Zheng and Y. Y. Zhang, *Acta Chim. Sin.*, 2023, **81**, 1402–1419.
34 E. De la Paz, N. H. Maganti, A. Trifonov, I. Jeerapan, K. Mahato, L. Yin, T. Sonsa-ard, N. Ma, W. Jung, R. Burns, A. Zarrinpar, J. Wang and P. P. Mercier, *Nat. Commun.*, 2022, **13**, 7405.
35 F. R. Chen, Z. K. Zhang, S. H. He, X. X. Yu and Y. X. Li, *J. Instrum. Anal.*, 2023, **42**, 150–157.
36 Z. F. Wan, N. T. Nguyen, Y. S. Gao and Q. Li, *Sustainable Mater. Technol.*, 2020, **25**, e00205.
37 M. Xia, H. D. Shao, Z. Huang, Z. Zhao, F. L. Jiang and Y. W. Hu, *IEEE Trans. Instrum. Meas.*, 2022, **71**, 1–9.
38 K. Settu, P. T. Chiu and Y. M. Huang, *Polymers*, 2021, **13**, 2795.
39 M. Guler, A. Zengin and M. Alay, *Anal. Biochem.*, 2023, **667**, 115091.
40 M. Cui, Z. M. Che, Y. H. Gong, T. D. Li, W. Hu and S. Wang, *Chem. Eng. J.*, 2022, **431**, 133455.
41 Y. Li, R. Han, X. H. Yu, M. Chen, Q. Q. Chao and X. L. Luo, *Sens. Actuators, B*, 2022, **373**, 132723.
42 A. Reda, S. A. El-Safty, M. M. Selim and M. A. Shenashen, *Biosens. Bioelectron.*, 2021, **185**, 113237.
43 G. Y. Wang, J. Y. Chen, L. Huang, Y. T. Chen and Y. X. Li, *Analyst*, 2021, **146**, 6631–6642.
44 B. Zhu, L. Yu, S. Beikzadeh, S. Zhang, P. Zhang, L. Wang and J. Travas-Sejdic, *Electrochim. Acta*, 2021, **378**, 138132.
45 R. Yang, W. Zhang, N. Tiwari, H. Yan, T. Li and H. Cheng, *Advanced Science*, 2022, **9**, 2202470.
46 K. Xia, W.-Y. Chiang, C. J. L. de la Rosa, Y. Fujita, S. Toyouchi, H. Yuan, J. Su, H. Masuhara, S. De Gendt, S. De Feyter, J. Hofkens and H. Uji-i, *Nanoscale*, 2020, **12**, 11063–11069.
47 S. B. Liu, X. H. Jiang, G. I. N. Waterhouse, Z. M. Zhang and L. M. Yu, *J. Electroanal. Chem.*, 2021, **897**, 115558.
48 B. C. Zhu, L. Yu, S. Beikzadeh, S. Y. Zhang, P. K. Zhang, L. Wang and J. Travas-Sejdic, *Electrochim. Acta*, 2021, **378**, 138132.
49 J. Zhu, S. Liu, Z. Hu, X. Zhang, N. Yi, K. Tang, M. G. Dexheimer, X. Lian, Q. Wang, J. Yang, J. Gray and H. Cheng, *Biosens. Bioelectron.*, 2021, **193**, 113606.
50 K. Settu, P. T. Chiu and Y. M. Huang, *Polymers*, 2021, **13**, 2795.
51 Y. X. Huang, Z. Y. Long, J. H. Zou, L. Z. Luo, X. Y. Zhou, H. Z. Liu, W. J. He, K. Shen and J. Wu, *IEEE Trans. Nanotechnol.*, 2022, **21**, 399–405.
52 Y. B. Hao, M. H. Fang, C. Xu, Z. Ying, H. Wang, R. Zhang, H. M. Cheng and Y. Zeng, *J. Mater. Sci. Technol.*, 2021, **66**, 57–63.
53 E. P. Aparicio-Martinez, A. Vega-Rios, V. Osuna and R. B. Dominguez, *Biosensors*, 2023, **13**, 207.
54 Y. Z. Huang, Y. K. Han, J. Y. Sun, Y. Zhang and L. Han, *Mater. Today Chem.*, 2022, **24**, 100895.
55 M. Srivastava, S. K. Srivastava, R. P. Ojha and R. Prakash, *Microchem. J.*, 2022, **182**, 107850.